Available online at www.sciencedirect.com

SciVerse ScienceDirect

Ceramics International 39 (2013) 2463–2471

CERAMICS INTERNATIONAL

www.elsevier.com/locate/ceramint

Enhanced performance of a macroporous ceramic support for nanofiltration by using α-Al_2O_3 with narrow size distribution

Hong Qi*, Shufeng Niu, Xiaoluo Jiang, Nanping Xu

State Key Laboratory of Materials-Oriented Chemical Engineering, Membrane Science and Technology Research Center, Nanjing University of Technology, Nanjing 210009, China

Received 12 August 2012; accepted 2 September 2012
Available online 8 September 2012

Abstract

Enhanced performance of a macroporous disk alumina support was fabricated through colloidal filtration route, by using α-Al_2O_3 powder with an average particle size of 1.1 μm. The support, sintered at 1250 °C, showed relative high permeances towards water (101 L h^{-1} m^{-2} bar^{-1}) and nitrogen (~2×10^{-6} mol m^{-2} s^{-1} Pa^{-1}), with an average surface roughness of ~175 nm and a high mechanical strength of 61.1 MPa. Titania supported γ-Al_2O_3 mesoporous layers were deposited onto this promising disk α-Al_2O_3 support through dip-coating. The disk membrane A1100/TiO_2/γ-Al_2O_3, with pore size of ca. 4.4 nm, showed a pure water flux as high as 4.5 L m^{-2} h^{-1} bar^{-1}, which is four times higher than that of γ-Al_2O_3 membrane reported in literature. This mesoporous membrane showed relative high retention rate (~80%) towards di-valent cations like Ca^{2+}, Mg^{2+}, but not for the mono-valent cation (Na^{+}).

Keywords: Ceramic membranes; Macroporous alumina support; Nanofiltration; Permeability

1. Introduction

As a pressure-driven membrane process without phase transition, nanofiltration (NF) membrane processes are widely used in separation, refinement and condensation that are ubiquitously present in process industry like water-treatment, pigment, food, paper-making, pharmacy and chemical engineering [1]. This new technology has gained much more attention due to its simple process without heating, no chemical reaction and is environmental friendly. The membrane materials, used in NF processes can be categorized into polymeric membranes and ceramic ones, of which polymeric nanofiltration membranes are commercially available for many years [2,3]. Nevertheless, polymeric NF membrane that can be applied under extreme conditions (e.g. lower or higher pH, aggressive organic chemicals) remains one of the main challenges in this field of membrane research [2]. In comparison with polymeric membranes, ceramic membranes have distinct advantages such as chemical, thermal and mechanical stability, which are suitable for application under harsh environments [4]. However, the fabrication of ceramic membranes is much more complicated than that of its organic counterpart [3], which severely limits implementation. Ceramic membranes are typically fabricated with an asymmetric layered structure consisting of support, intermediate layers and top layer, which fulfils the separation process [5]. At present, much more investigations are focused on the development of NF membrane materials, including γ-Al_2O_3, TiO_2, ZrO_2 and HfO_2 [3,6–16], of which TiO_2 is commercially available by Inopor, Germany. With respect to fabrication of ceramic NF membranes, porous alumina materials are normally used as support providing a pore size in the range of 1–10 μm, which require 2–5 subsequent intermediate layers to reduce support pore size and roughness, so as to facilitate NF membrane deposition [4]. Each layer must separately undergo a drying and sintering step, which inevitably hampers implementation of ceramic NF membranes for large amounts of potential applications.

To optimize the support structure in such a way that it is suitable for the formation of NF membranes in one subsequent step, a high quality alumina powder with narrow particle size distribution was used to fabricate supports

*Corresponding author. Tel.: +86 25 83172279; fax: +86 25 83172292.
E-mail address: hqinjut@yahoo.com.cn (H. Qi).

0272-8842/$ - see front matter © 2012 Elsevier Ltd and Techna Group S.r.l. All rights reserved.
http://dx.doi.org/10.1016/j.ceramint.2012.09.004

Nomenclature

Q	support/membrane permeance (L m^{-2} h^{-1} bar^{-1})
m	weight of the permeate (Kg)
A	effective filtration area (m^2)
t	filtration time (h)
Δp	trans-membrane pressure (bar)
ρ	density of the permeate solution (Kg/dm^3)
R_f	three point bending strength of the support (MPa)
P	fracture stress (N)
L	distance between supporting jigs (mm)
B	width of the sample at fracture point (mm)
h	height of the sample at fracture point (mm)
R	ionic retention rate of the membrane
C_{ip}	ionic concentration of permeate solution (mol L^{-1})
C_{if}	ionic concentration of feed solution (mol L^{-1})
r	PEG radius (Å)
M_W	90% MWCO of PEG for membrane (g mol^{-1})

possessing a homogeneous pore structure, with an average pore size of ~100 nm [17]. Supports prepared from stabilized suspensions of Sumitomo AKP30 (with a mean particle size of ~400 nm) exhibited ideal surface morphology (with an average roughness of ~30 nm) and excellent mechanical strength (> 200 MPa), but inadequate permeability for gases (e.g. the permeance for N_2 was $\sim 5.15 \times 10^{-7}$ mol m^{-2} s^{-1} Pa^{-1}) [17], and liquids (e.g. the permeance for water was 3.3 L m^{-2} h^{-1} bar^{-1}) [18]. Alumina with an average particle size of ~600 nm, was used to fabricate a more permeable support [17,19]. However, liquid permeance was still not high enough (4.5 L m^{-2} h^{-1} bar^{-1}). Although the NF membrane processes are generally carried out at higher pressure of 10–20 bar, those low permeances for ceramic NF membranes still cannot meet the requirements for industrial implementation. To improve the permeability of ceramic NF membranes, further optimization of the preparation procedures of NF separation layers (including hydrolysis and condensation of precursors, dip-coating, drying and calcination processes) is required. On the other hand, it is well known that high quality porous supports are essential for NF membranes. Therefore, optimizing support structures, reduction of the amount of intermediate layers, is another way to improve the permeability of NF membranes. With respect to the latter strategy to improve the permeance of ceramic NF membranes, research progress can be summarized as follows. First of all, coarse alumina with a mean size as large as 3 μm was adopted to fabricate supports [17], which showed much higher gas permeability in the order of ~ $\times 10^{-5}$ mol m^{-2} s^{-1} Pa^{-1}. Secondly, supports with gradient structures were prepared through a single-step processing method, by using powders with relative broad size distributions [20–22]. Highly porous structure with a continuously increasing mean pore size from top to bottom was obtained by a controlled sedimentation technique. Results showed that those functionally gradient supports exhibited pure water permeance as high as 25.2 L m^{-2} h^{-1} bar^{-1}, with top layer pore size less than 50 nm was achieved. However, neither liquid permeances of supports nor subsequent NF membrane fabrication was reported in the above-mentioned research.

In this paper, we report on the fabrication of a high performance macroporous support, starting from alumina powder with an average size of 1.1 μm. Such alumina particles would result in relative large pore size of the partially sintered porous structure and, hence, improve permeance of the macroporous support. On the other hand, the relatively narrow particle size distribution induces a surface morphology that enables the reduction of defects in subsequently deposited NF membrane layers. The effect of sintering temperature on properties of this promising support, as well as that properties in comparison with the data cited from references, was investigated in detail. Nanofiltration properties of γ-Al_2O_3 mesoporous membrane, which is deposited on this promising support, were also reported.

2. Experimental

2.1. Preparation of macroporous alumina supports

α-Al_2O_3 powder (purity > 99.5%, Nanjing, China) with a mean particle size of ca. 1.1 μm, were used as received. 75 g α-Al_2O_3 powder was introduced into 175 g deionized water under stirring and pH value of the suspension was adjusted to 1.5 with the addition of 1 mol L^{-1} HNO_3. Subsequently, the suspension was poured into a dedicated glass bottle and ultrasonically dispersed for 20 min (VC 505, Sonics and Materials Inc.). After screening with a stainless-steel sieve (mesh size: 0.1 mm), 25 ml well-dispersed suspension was casted into a PTFE (polytetrafluoroethylene) disk module followed by free gravitative sedimentation for 4 h. Subsequently vacuum-pumping was adopted to suck the suspension for 30 min to obtain green disk-shaped alumina compacts. The samples were dried overnight and then sintered in air in the temperature range of 1100–1400 °C, with dwelling time and ramping rate being 2 h and 2 °C/min, respectively. The sintered supports, hereafter referred to as support A1100, were polished with a polishing apparatus (Phoenix 4000, Buehler) equipped with diamond abrasive disc, so as to provide smooth surfaces for subsequent membranes deposition.

2.2. Preparation of titania intermediate and γ-Al_2O_3 top layers

A TiO_2 colloidal sol with an average particle size of 41.3 nm, was fabricated through an acid-catalyzed colloidal

sol–gel route, by using titanium isopropoxide as a precursor. The sol with suitable viscosity was deposited onto the above-mentioned disk α-Al_2O_3 support *via* dip-coating method with a dedicated apparatus (MEMDIP 5, Pervatech B.V., The Netherlands). This α-Al_2O_3 supported TiO_2 intermediate layer was dried and then calcined at 500 °C. The same procedure was reproduced for one more time in order to repair the defects in the support. The objective for deposition of TiO_2 intermediate layer onto the α-Al_2O_3 support was to reduce the pore size of the support underneath and, hence, facilitates the top γ-Al_2O_3 mesoporous layers formation. A stable Boehmite sol with a mean particle size of about 20 nm was synthesized by using aluminum sec-butoxide as a precursor through particle colloidal sol–gel route. The Boehmite sol was coated onto α-Al_2O_3 supported TiO_2 intermediate layer through dip-coating, followed by drying and calcining (500 °C) to form a γ-Al_2O_3 membrane. The membrane was hereafter referred to as A1100/TiO_2/γ-Al_2O_3.

2.3. Materials characterization

The particle size distribution of alumina powder was probed by using a Zetatrac analyzer (Microtrac Inc. US). The densification curve of the support, represented as the linear shrinkage of the disk support, was calculated with the diameter variation of the support before and after sintering. Porosity of the macroporous support was determined by Archimedes method with water as immersion medium. Pore size distribution of support was measured by mercury intrusion method (Poremaster, Quantachrome). The smoothness of the disk support, characterized as surface roughness, was determined by a roughness-determination device (JB-4C, Taiming Optics Instrument Inc. Shanghai). Each measurement was carried out after polishing of the samples. Scanning electron microscope (SEM, JSM-6300, JEOL) was employed to observe surfaces and cross-section of disk-shaped supports. Pure water flux of disk support and membrane was characterized by using a dead-end filtration apparatus under trans-membrane pressure in the range of 1–5 bar, as shown in Fig. 1. The pure water flux was calculated with Eq. (1) as follows:

$$Q = \frac{m}{\rho A t \Delta p} \quad (1)$$

Where Q is the support/membrane permeance (L m^{-2} h^{-1} bar^{-1}), m is the weight of the permeate (Kg), A is the effective filtration area (m^2), t is the filtration time (h), Δp is the trans-membrane pressure (bar), and ρ is the density of the permeate solution (Kg/dm^3).

Single gas permeability of the disk-shaped support, characterized by its nitrogen permeance at ambient temperature, was measured by using a dead-end mode set-up. A disk-shaped support was sealed in a stainless steel module using fluoroelastomer O-rings. The pressure difference across the support was 1 bar, while the permeate side was vent to the atmosphere. The mechanical strength of the support, represented as three-point bending strength, was determined by a materials testing machine (CMT 6203, New SANS Inc. Shenzhen, China). A rectangular sample with size of 3.5 mm × 7 mm × 25 mm was set on two stainless-steel jigs 20 mm apart (see Fig. 2). Samples were bent and fractured by an upper stainless-steel jig, at a constant loading rate of 0.5 mm/min. The three-point bending strength of supports was calculated by the following Eq. (2):

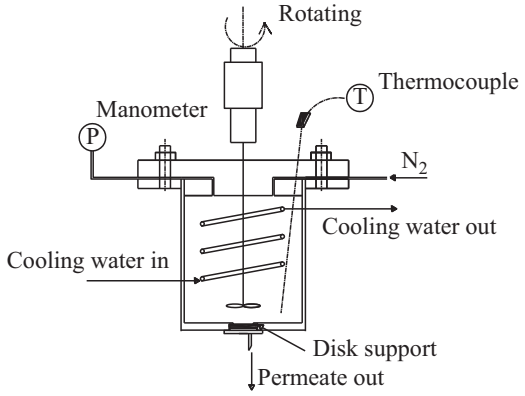

Fig. 1. Schematic diagram of a dead-end filtration apparatus for the determination of pure water flux of disk support and membrane.

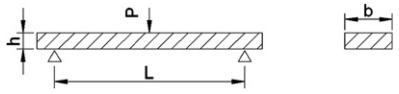

Fig. 2. Schematic diagram of the apparatus for the determination of mechanical strength of rectangular macroporous support.

$$R_f = \frac{3PL}{2bh^2} \quad (2)$$

Where R_f is the three point bending strength (MPa), P is the fracture stress (N), L is the distance between supporting jigs (mm), b is the width of the sample at fracture point (mm), h is the height of the sample at fracture point (mm).

Retention property of membrane A1100/TiO_2/γ-Al_2O_3 was characterized by a dead-end filtration mold using the same apparatus, as depicted in Fig. 1, while the feed solution was kept stirring at a speed of 200 r/min to avoid concentration gradient. The feed solution contained PEGs (Alfa Aesar) with molecular masses of 4000, 10,000, 20,000, and 100,000, while the concentration was 3 g L^{-1}. The measurements were conducted at a trans-membrane pressure of 4 bar and a temperature of 20 ± 3 °C. The retention rates of the membrane were determined with gel permeation chromatography (GPC, Waters), by collecting both feed and permeate solutions. The molecular mass of the PEG corresponding to a 90% retention level was taken as the MWCO (molecular weight cut-off) of the membrane. Ionic retention properties of the mesoporous membrane A1100/TiO_2/γ-Al_2O_3 towards single component salt solutions, like NaCl, $CaCl_2$, Na_2SO_4 and $MgCl_2$, were also determined by using a disk dead-end filtration apparatus, with the same procedures as the PEG retention

measurement. The concentration of the above-mentioned solutions was controlled in the range of 0.005–0.1 mol L^{-1}. And the pH was modulated with the addition of HNO_3 and $NH_3 \cdot H_2O$, respectively. Ionic retention rates of the membrane were determined by measuring conductivities of the solutions, which were collected from both feed and permeate side, and calculated with Eq. (3) as follows:

$$R(\%) = \left(1 - \frac{C_{ip}}{C_{if}}\right) 100 \quad (3)$$

Where R is the ionic retention rate of the membrane, C_{ip} is the ionic concentration of permeate solution, and C_{if} is the ionic concentration of feed solution.

3. Results and discussion

3.1. Properties of macroporous alumina support as a function of sintering temperature

Fig. 3 shows the particle size distribution of α-Al_2O_3 powders used in this study. It was found that the alumina particle size was in the range of 0.7 –2 μm, with an average size of ~1.1 μm. It should be noted that a small amount of particles, with size smaller than 0.5 μm, can also be observed in Fig. 3. The narrow particle size distribution is a prerequisite for the formation of a uniform microstructure, which is obtained through random packing of solid particles. Fig. 4 gives the linear shrinkage of support A1100 as a function of sintering temperature. Also shown in Fig. 4 for comparison, are shrinkage data [19] of a macroporous support (hereafter referred to as support A400), which is fabricated by using α-Al_2O_3 powders with an average size of 400 nm (Sumitomo AKP-30). It is visible that the linear shrinkage of support A1100 increased as the sintering temperature elevated, from 0.91% (1100 °C) to 12% (1350 °C). Under the same sintering conditions, support A400 exhibited higher shrinkage rate in comparison with that of support A1100, which is due to the fine-grained (400 nm) alumina used for fabrication of the support A400. However, it is worthwhile to note that

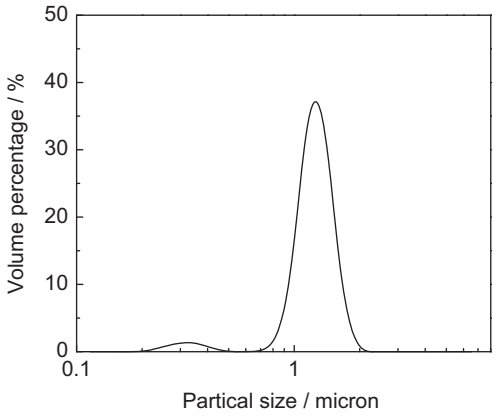

Fig. 3. Particle size distribution of alumina powder used in this study.

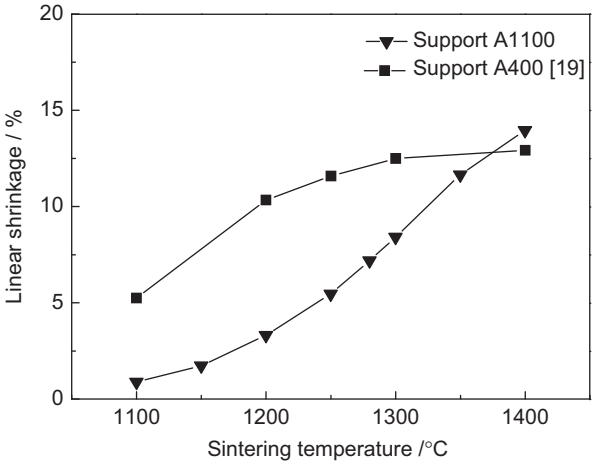

Fig. 4. Linear shrinkage of support A1100 as a function of sintering temperature. Also shown are data of support A400 (cited from reference [19]).

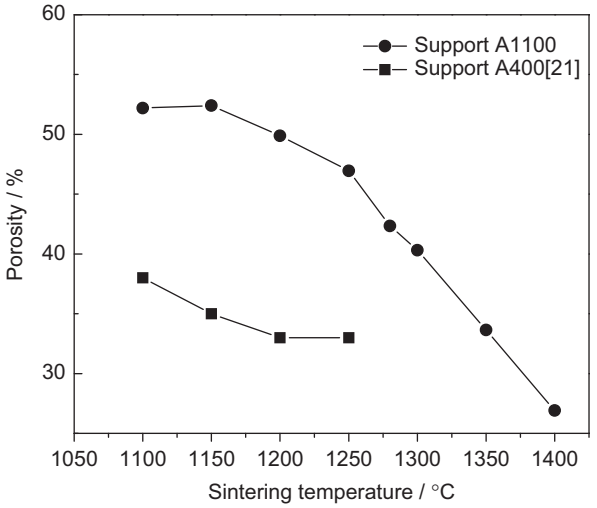

Fig. 5. Sintering temperature dependence of porosity of support A1100. Also shown are porosity of support A400 sintered at different temperatures, which are cited from reference [21].

support A1100 sintered at 1400 °C showed a higher shrinkage than that of support A400 sintered at the same temperature. It might be the case that a small fraction of sub-micrometer alumina particles accelerated the sintering rate of support A1100, when the sintering temperature was higher than 1350 °C. On the other hand, a much more homogeneous support A400 [19], prepared from more evenly-graded alumina AKP30, should be responsible for the lower shrinkage.

The porosity of support A1100 as a function of the sintering temperature, as well as porosity of support A400 cited from reference [21], are given in Fig. 5. It can be seen that the porosity of support A1100 decreased with sintering temperature, from 52.2% (1100 °C) to 26.9% (1400 °C). The same variation tendency is observed for support A400. However, it should be noted that the porosity of support

A400 sintered in the temperature range of 1100 °C–1250 °C was always below 40%, which is lower than that of support A1100. The much higher porosity of support A1100 can be a result of reduced packing density of particles, which exhibit a broad size distribution. Fig. 6 shows sintering temperature dependence of pure water flux of support A1100. It was found that support A1100 sintered at both 1200 °C and 1250 °C showed permeances as high as 100–105 L m^{-2} h^{-1} bar^{-1}. In comparison with that of support A400 sintered at similar temperatures, the permeance of support A1100 was two orders of magnitude higher than that of support A400 [21], as displayed in Fig. 6. A remarkable reduced pure water flux of 43 L m^{-2} h^{-1} bar^{-1} for support A1100 was observed as the sintering temperature reached 1350 °C. Nevertheless, in comparison with that of support A 400, a much higher pure water flux of 36 L m^{-2} h^{-1} bar^{-1} was maintained when the sintering temperature of support A1100 was as high as 1400 °C. By comparison with Fig. 5 and Table 1, it is obvious that both pore size and porosity have impact on pure water flux of the support. Trans-membrane pressure dependence of pure water flux for both support A1100 (sintered at 1200 °C) and support A400 (sintered at 1100 °C) [18] are displayed in Fig. 7. As seen in this figure, pure water flux for both support A1100 and support A400 exhibited linear relationship with pressure, which suggests a pressure-driven membrane process. The much higher water permeance for support A1100 can be attributed to its higher porosity and pore size, as evidenced by Fig. 5 and Table 1, respectively.

Fig. 8 shows three point bending strengths of supports A1100 sintered at different temperatures. The mechanical strength of support A1100 increased from 7.7 MPa to 184 MPa, as the sintering temperature elevated from 1100 °C to 1400 °C. As is well known that the sintering of the porous alumina support is a solid-state process and lies in the initial stage, which is controlled by the surface diffusion mechanism [23]. The higher sintering temperature

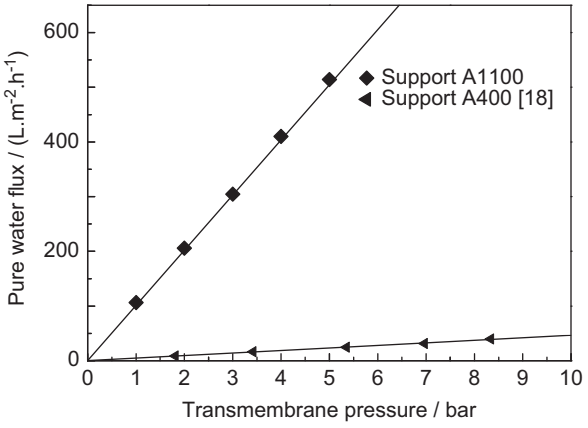

Fig. 7. Comparison of pure water flux of support A1100 fabricated in this work with that of support A400 (cited from reference [18]).

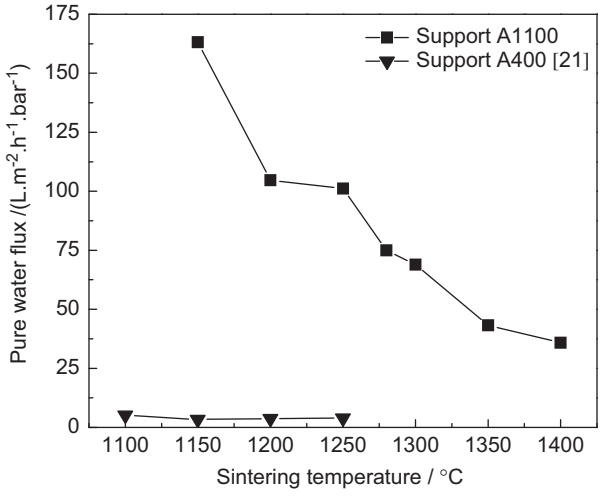

Fig. 6. Sintering temperature dependence of pure water flux of support A1100. Also shown are pure water flux of support A400 sintered at various temperatures, which are cited from reference [21].

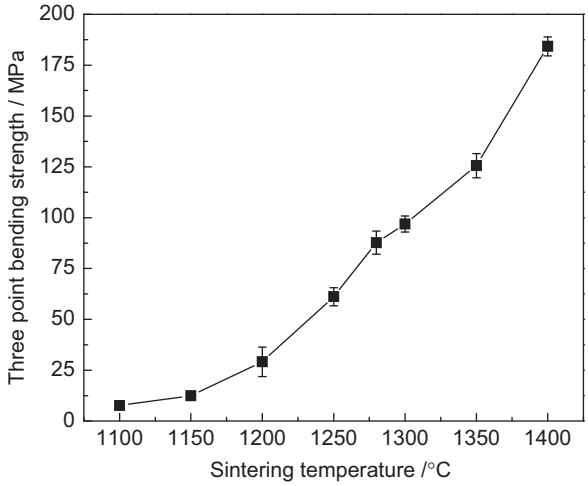

Fig. 8. Three point bending strength of support A1100 as a function of sintering temperature.

Table 1
Comparison of properties of support A1100 fabricated in this work with that of support A400 (cited from reference [17]).

α-Al_2O_3 support	Powder size (nm)	Pore size (nm)	Porosity (%)	Average roughness (nm)	Mechanical strength (MPa)	Pure water flux (L m^{-2} h^{-1} bar^{-1})
A400 [17]	400	~70	~35	~30	> 100	4.5
A1100 (this work)	1100	~250	~47	~175	61.1	101

results in a higher diffusion coefficient and, hence, accelerates sintering. The improvement of the mechanical strength of support A1100 can be assigned to the increase in neck area between alumina particles with increasing sintering temperature, as evidenced by Fig. 9. Fig. 9 shows cross-sectional SEM photos of support A1100 sintered at 1100 °C, 1250 °C and 1350 °C, respectively. The 1100 °C-sintered support A1100 showed a low three point bending strength of approximately 8 MPa because alumina particles with size of 0.5–2 μm, aggregated in its original state, as can be found in Fig. 9. Alumina particles impinged onto each other and obvious necks were formed as the sintering temperature increased. When the sintering temperature reached 1350 °C, a more dense-packed microstructure of support A1100, with the concomitant growth of the necks between alumina particles, can be observed. As a result, the three point bending strength of support A1100 reached as high as 126 MPa when the sintering temperature was 1350 °C.

Fig. 10 gives the SEM surface photo of support A1100, which is sintered at 1250 °C. It can be seen that the surface of the support A1100 was smooth without any defects or cracks, showing the measured surface roughness of ~175 nm (see Table 1). The pore size distribution of support A1100 sintered at 1250 °C, measured with mercury porosimetry method, is given in Fig. 11. It can be seen that the support A1100 provided a narrow pore size distribution in the range of 0.1–1 μm, with an average pore size of approximately 250 nm.

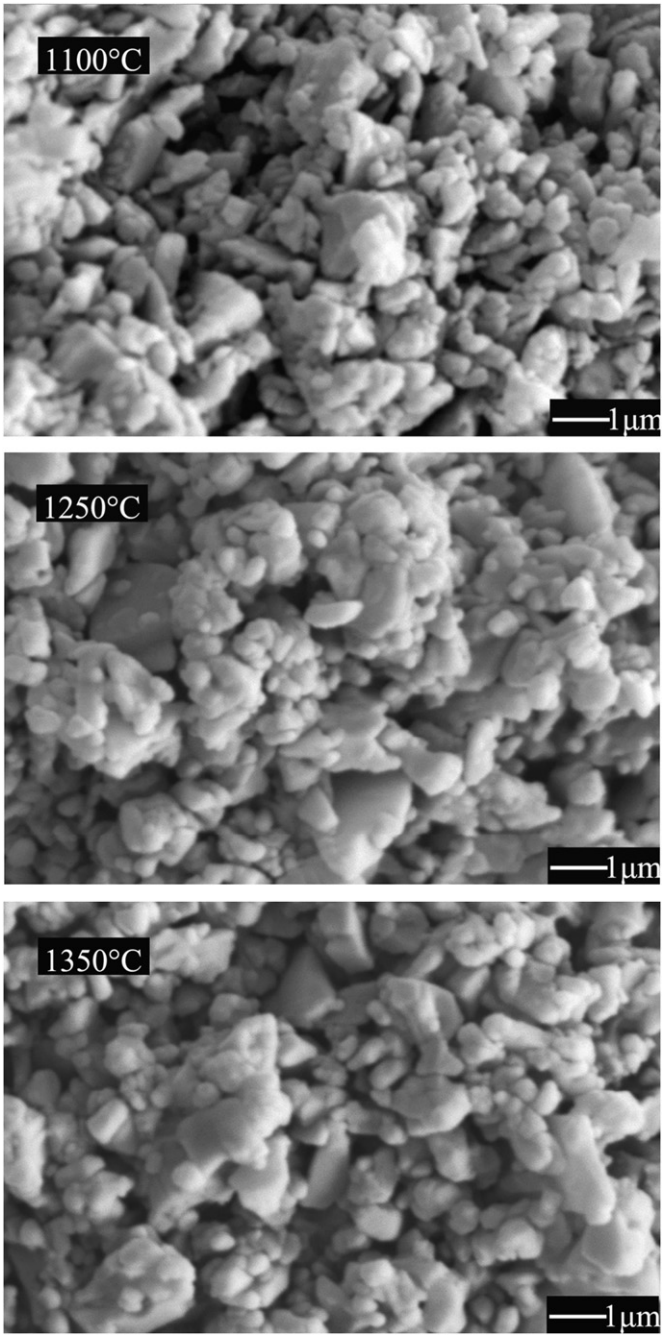

Fig. 9. SEM sectional photos of support A1100 sintered at 1100 °C, 1250 °C and 1350 °C, respectively.

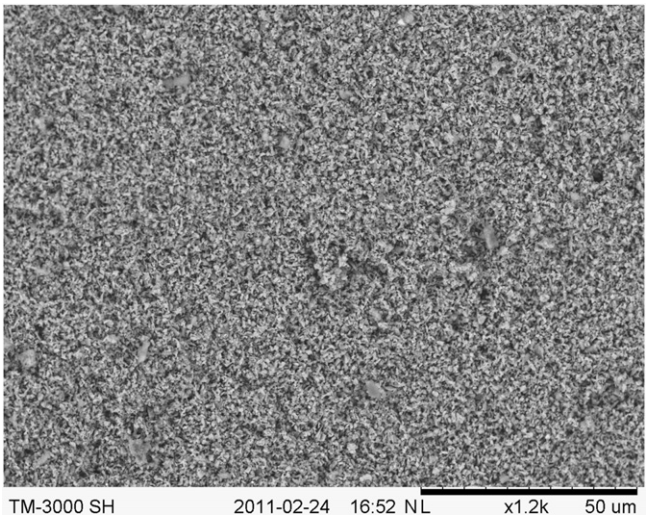

Fig. 10. SEM photo of surface of support A1100 sintered at 1250 °C.

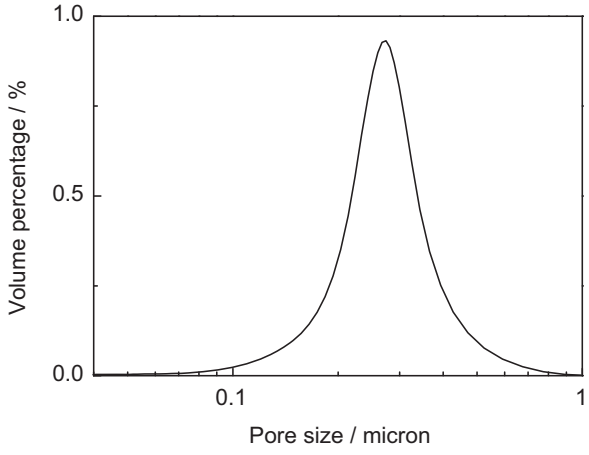

Fig. 11. Pore size distribution of disk macroporous α-Al_2O_3 support sintered at 1250 °C, as measured by mercury porosimeter method.

According to the above investigations, the macroporous support A1100 sintered at 1250 °C provided with integrated properties of permeability, mechanical strength and surface roughness, as shown in Table 1. Also shown in Table 1 for comparison, are properties of support A400, which are cited from reference [17]. As can be seen in Table 1, support A1100 exhibited much higher pure water flux than that of support A400. More important, the N_2 permeance for a 2 mm-thick support A1100, measured at ambient temperature, was up to $\sim 2 \times 10^{-6}$ mol m^{-2} s^{-1} Pa^{-1}, which is approximately four times higher than that of support A400 [17]. It was reported that the Boehmite layer can be applied on a support, whose average roughness is smaller than 300 nm [4]. Therefore, γ-Al_2O_3 mesoporous membrane deposited onto this promising support is anticipated, although the surface roughness of support A1100 is larger than that of support A400.

3.2. Properties of A1100/TiO_2/γ-Al_2O_3 mesoporous membrane

Fig. 12 illustrates the PEG retention curve for disk A1100/TiO_2/γ-Al_2O_3 mesoporous membrane. It was found that the 90% MWCO of PEG for A1100/TiO_2/γ-Al_2O_3 membrane was 7450 g mol^{-1}, which can be used to calculate the PEG radius based on the correlation between molecular weight of PEG and its Stokes–Einstein radius [6], as shown in Eq. (4).

$$r = 0.262 \times (M_W)^{0.5} - 0.3 \quad (4)$$

Where r is the PEG radius (Å), M_W is the 90% MWCO of PEG for membrane (g mol^{-1}).

According to Eq. (4), the retained molecular size was roughly 4.4 nm. Therefore, the pore size of the membrane A1100/TiO_2/γ-Al_2O_3 was 4.4 nm at the most, so as to allow complete retention of PEG. The pure water flux of membrane A1100/TiO_2/γ-Al_2O_3 fabricated in this paper, together with that of membrane A400/γ-Al_2O_3 cited from reference [18,24], is compared in Table 2. It should be noted that although the water permeance of support A1100 was much higher (two orders of magnitude higher) than that of support A400, while the pure water flux of γ-Al_2O_3 membrane fabricated in this study was only four times higher than that of membrane A400/γ-Al_2O_3 reported in literatures [18,24]. Salt retention measurements of membrane A1100/TiO_2/γ-Al_2O_3 fabricated in this study, with respect to NaCl, Na_2SO_4, $MgCl_2$ and $CaCl_2$, are displayed in Figs. 13–15.

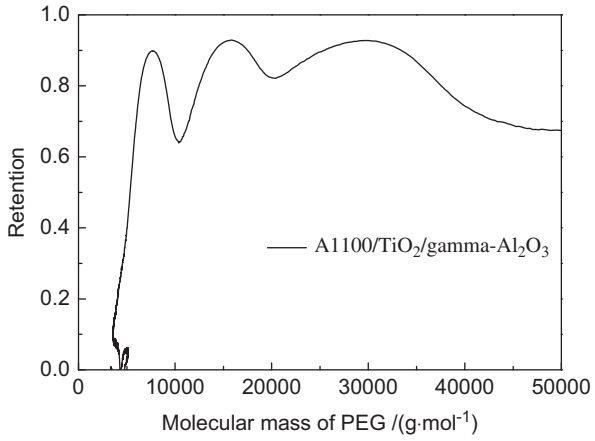

Fig. 12. Molecular weight cut-off (MWCO) of PEG for mesoporous membrane A1100/TiO_2/γ-Al_2O_3 calcined at 500 °C.

Table 2
Comparison of pure water flux of membrane A1100/TiO_2/γ-Al_2O_3 fabricated in this work with that of membrane A400/γ-Al_2O_3 (cited from references [18,24]).

	Support A 400	Membrane A400/ γ-Al_2O_3	Support A 1100 (this work)	Membrane A1100/TiO_2/ γ-Al_2O_3 (this work)
Pure water flux (L m^{-2} h^{-1} bar^{-1})	4.5	1.1	101	4.5

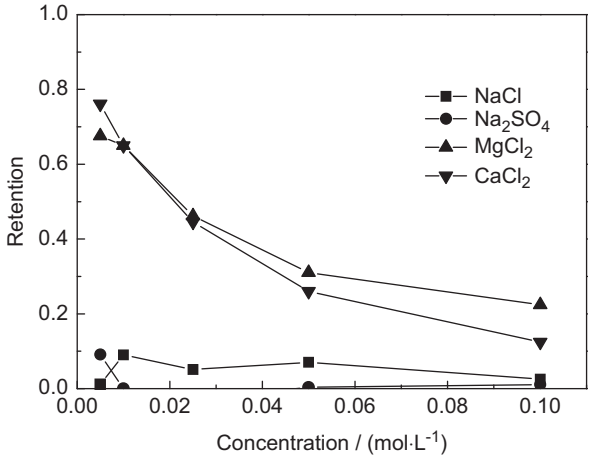

Fig. 13. Concentration dependence of retention properties for mesoporous membrane A1100/TiO_2/γ-Al_2O_3 with respect to NaCl, Na_2SO_4, $MgCl_2$ and $CaCl_2$.

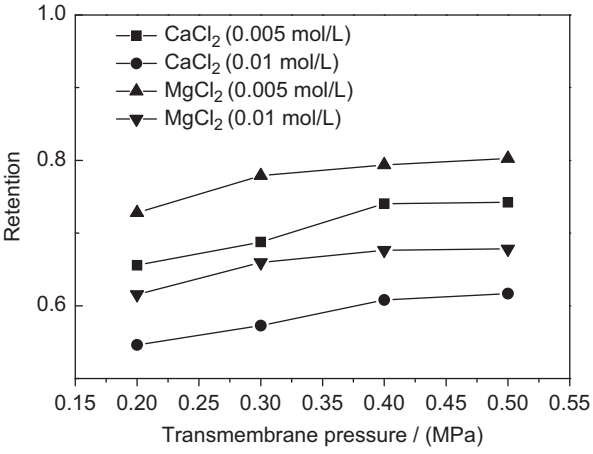

Fig. 14. Pressure dependence of retention properties for mesoporous membrane A1100/TiO_2/γ-Al_2O_3 with respect to $MgCl_2$ and $CaCl_2$.

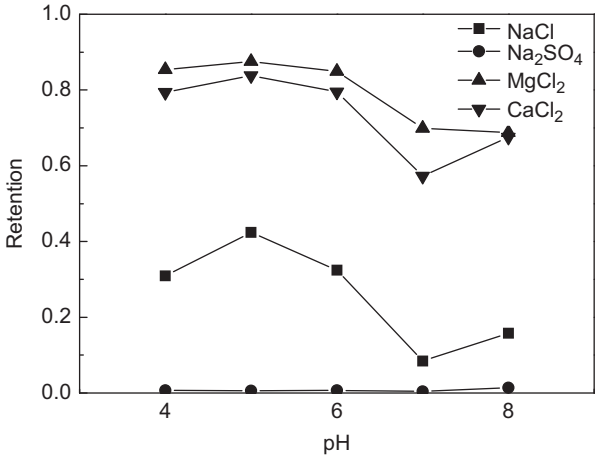

Fig. 15. Retention properties of membrane A1100/TiO_2/γ-Al_2O_3 as a function of pH.

Fig. 13 gives ionic retentions of the membrane A1100/TiO_2/γ-Al_2O_3 as a function of the feed concentration, with respect to single salt solutions, like NaCl, Na_2SO_4, $MgCl_2$ and $CaCl_2$. All filtration measurements were conducted at pH = 6 and a trans-membrane pressure of 4 bar. In concentration range of 0.005–0.1 mol L^{-1}, the membrane A1100/TiO_2/γ-Al_2O_3 exhibited higher retention rates towards di-valent cations (*i.e.* Mg^{2+}, Ca^{2+}) than that of the mono-valent cation (Na^+), which is the characteristic of NF membranes. The decreased retention rate in the order of $MgCl_2 > NaCl > Na_2SO_4$, can be explained on the basis of the Donnan exclusion mechanism [25]. Fig. 13 also displays decreased retention rate towards single component salt with concentration. This can be explained by the decreased thickness of the electric double layer with increased salt concentration (*i.e.* higher ionic strength) and, hence, resulted in lower retention rate.

Fig. 14 shows retention rates regarding $CaCl_2$ and $MgCl_2$ as a function of trans-membrane pressure. As can be seen in Fig. 14, the retention rate increased with the pressure and reached a plateau in the end. The results line up with observations made by Schaep et al. [26], showing the transport of ions through membrane includes convection, diffusion and electro migration, which are determined by the trans-membrane pressure.

Fig. 15 illustrates the retention rates of A1100/TiO_2/γ-Al_2O_3 membrane towards NaCl, Na_2SO_4, $MgCl_2$ and $CaCl_2$ solutions, as a function of pH. It can be seen that the minimum retentions for each salt solution can be found around a pH value of 7.0. This behavior can be explained by iso-electric point of γ-Al_2O_3 membrane, which is at a pH value of 7.5 [26]. As is well known, the separation mechanisms for NF membranes are based on both micropore sieving and charged membrane surfaces. At pH values around 7.5, the separation of γ-Al_2O_3 membrane regarding ionic only relies on sieving effect because of the uncharged membrane surfaces. Therefore, the minimum retention rates can be expected if the relative large membrane pore size of ~4.4 nm is taken into account.

4. Conclusions

(1) A macroporous alumina support was fabricated through a colloidal filtration route, by using α-Al_2O_3 powders with an average particle size of 1.1 μm. At a sintering temperature of 1250 °C, support A1100 with integrated performances of permeability, mechanical strength and surface roughness was obtained. This support provided relative high permeances towards water (101 L h^{-1} m^{-2} bar^{-1}) and nitrogen (~2 × 10^{-6}mol m^{-2} s^{-1} Pa^{-1}), while maintained an average surface roughness of ~175 nm and a sufficient mechanical strength (61.1 MPa), which is promising for NF membrane formation.

(2) A γ-Al_2O_3 mesoporous layer was deposited onto α-Al_2O_3 supported TiO_2 intermediate layer through dip-coating. The membrane A1100/TiO_2/γ-Al_2O_3, with pore size of approximately 4.4 nm, showed a pure water flux as high as 4.5 L m^{-2} h^{-1} bar^{-1}. This mesoporous membrane exhibited relative high retention rate (~80%) towards di-valent cations like Ca^{2+} and Mg^{2+}, but not for the mono-valent cation (Na^+).

Acknowledgments

The authors would like to thank the financial support from the National Natural Science Foundation of China (20906047, 21276123), the National High Technology Research and Development Program of China (2012AA03A606), State Key Laboratory of Materials-Oriented Chemical Engineering (ZK201002), the Natural Science Research Plan of Jiangsu Universities (11KJB530006) and the "Summit of the Six Top Talents" Program of Jiangsu Province.

References

[1] R. Mallada, M. Menéndez, Inorganic Membranes Synthesis, Characterization and Applications, Elsevier Press, Amsterdam, The Netherlands, 2008, pp. 177–216.
[2] P. Vandezande, L.E.M. Gevers, I.F.J. Vankelecom, Solvent resistant nanofiltration: separating on a molecular level, Chemical Society Reviews 37 (2) (2008) 365–405.
[3] T. Van Gestel, H. Kruidhof, D.H.A. Blank, H.J.M. Bouwmeester, ZrO_2 and TiO_2 membranes for nanofiltration and pervaporation—Part 1. Preparation and characterization of a corrosion-resistant ZrO_2 nanofiltration membrane with a MWCO < 300, Journal of Membrane Science 284 (1–2) (2006) 128–136.
[4] A.J. Burggraaf, L. Cot, Fundamentals of Inorganic Membrane Science and Technology, Elsevier Press, Amsterdam, The Netherlands, 1996.
[5] L.L. Zhang, I.-S. Park, K. Shqau, W.S. Winston Ho, H. Verweij, Supported inorganic membranes: promises and challenges, Journal of the Minerals Metals and Materials Society 61 (4) (2009) 61–71.
[6] P. Puhlfürβ, A. Voigt, R. Weber, M. Morbe, Microporous TiO_2 membranes with a cut off < 500 Da, Journal of Membrane Science 174 (1) (2000) 123–133.

[7] J. Etienne, A. Larbot, A. Julbe, L. Cot, A microporous zirconia membrane prepared by the sol–gel process from zirconyl oxalate, Journal of Membrane Science 86 (1–2) (1994) 95–102.
[8] R. Vacassy, C. Guizard, V. Thoraval, L. Cot, Synthesis and characterization of microporous zirconia powders: application in nanofilters and nanofiltration characteristics, Journal of Membrane Science 132 (1) (1997) 109–118.
[9] T. Van Gestel, C. Vandecasteele, A. Buekenhoudt, C. Dotremont, J. Luyten, R. Leysen, B. Van der Bruggen, G. Maes, Alumina and titania multilayer membranes for nanofiltration: preparation, characterization and chemical stability, Journal of Membrane Science 207 (1) (2002) 73–89.
[10] T. Van Gestel, C. Vandecasteele, A. Buekenhoudt, C. Dotremont, J. Luyten, R. Leysen, B. Van der Bruggen, G. Maes, Salt retention in nanofiltration with multilayer ceramic TiO_2 membranes, Journal of Membrane Science 209 (2) (2002) 379–389.
[11] J. Sekulic, J.E. ten Elshof, D.H.A. Blank, A microporous titania membrane for nanofiltration and pervaporation, Advanced Materials 16 (17) (2004) 1546–1550.
[12] T. Tsuru, D. Hironaka, T. Yoshioka, M. Asaeda, Titania membranes for liquid phase separation: effect of surface charge on flux, Separation and Purification Technology 25 (1–3) (2001) 307–314.
[13] T. Tsuru, D. Hironaka, T. Yoshioka, M. Asaeda, Effect of divalent cations on permeate volume flux through porous titania membranes, Desalination 147 (1–3) (2002) 213–216.
[14] I. Voigt, G. Fischer, P. Puhlfürβ, M. Schleifenheimer, M. Stahn, TiO_2–NF-membranes on capillary supports, Separation and Purification Technology 32 (1–3) (2003) 87–91.
[15] S. Benfer, U. Popp, H. Richter, C. Siewert, G. Tomandl, Development and characterization of ceramic nanofiltration membranes, Separation and Purification Technology 22–23 (2001) 231–237.
[16] P. Blanc, A. Larbot, J. Palmeri, M. Lopez, L. Cot, Hafnia ceramic nanofiltration membranes. Part I: preparation and characterization, Journal of Membrane Science 149 (2) (1998) 151–161.
[17] M.L. Mottern, W.V. Chiu, Z.T. Warchol, K. Shqau, H. Verweij, High-performance membrane supports: a colloidal approach to the consolidation of coarse particles, International Journal of Hydrogen Energy 33 (14) (2008) 3903–3914.
[18] S.R. Chowdhury, R. Schmuhl, K. Keizer, J.E. ten Elshof, D.H.A. Blank, Pore size and surface chemistry effects on the transport of hydrophobic and hydrophilic solvents through mesoporous γ-alumina and silica MCM-48, Journal of Membrane Science 225 (1–2) (2003) 177–186.
[19] K. Shqau, M.L. Mottern, D. Yu, H. Verweij, Preparation and properties of porous α-Al_2O_3 membrane supports, Journal of the American Ceramic Society 89 (6) (2006) 1790–1794.
[20] C. Falamaki, J. Veysizadeh, Comparative study of different routes of particulate processing on the characteristics of alumina functionally graded microfilter/membrane supports, Journal of Membrane Science 280 (1–2) (2006) 899–910.
[21] K. Darcovich, D. Roussel, F.N. Toll, Sintering effects related to filtration properties of porous continuously gradient ceramic structures, Journal of Membrane Science 183 (2) (2001) 293–303.
[22] K. Darcovich, C.R. Cloutier, Processing of functionally gradient ceramic membrane substrates for enhanced porosity, Journal of the American Ceramic Society 82 (8) (1999) 2073–2079.
[23] W.D. Kingery, H.K. Bowen, D.R. Uhlmann, Introduction to Ceramics, 2nd ed., John Wiley and Sons, Inc, 1976.
[24] J. Sekulic, A. Magraso, J.E. ten Elshof, D.H.A. Blank, Influence of ZrO_2 addition on microstructure and liquid permeability of mesoporous TiO_2 membranes, Microporous and Mesoporous Materials 72 (1–3) (2004) 49–57.
[25] J.M.M. Peeters, M.H.V. Mulder, H. Strathmann, Streaming potential measurements as a characterization method for nanofiltration membranes, Colloids and Surfaces A: Physicochemical and Engineering Aspects 150 (1–3) (1999) 247–259.
[26] J. Schaep, C. Vandecasteele, B. Peeters, J. Luyten, C. Dotremont, D. Roels, Characteristics and retention properties of a mesoporous γ-Al_2O_3 membrane for nanofiltration, Journal of Membrane Science 163 (2) (1999) 229–237.